International Journal of Heat and Technology
Vol. 40, No. 1, February, 2022, pp. 273-281
Journal homepage: http://iieta.org/journals/ijht

Heat Transfer and Pressure Drop Performance of a Hydraulic Mining Shovel Radiator by Using Ethylene Glycol/Water-Based Al_2O_3 Nanofluids

José Canazas*, Oleg Kamyshnikov

School of Mechanical Engineering, Universidad Nacional de San Agustin de Arequipa, Arequipa 04000, Peru

Corresponding Author Email: jcanazas@unsa.edu.pe

https://doi.org/10.18280/ijht.400132

Received: 13 January 2022
Accepted: 17 February 2022

Keywords:
heat transfer, hydraulic mining shovel, nanofluids, pressure drop, radiator

ABSTRACT

Nanofluids are excellent replacements for vehicle radiator coolants and they have the ability to significantly enrich the performance of vehicle radiators. A numerical study of thermal and hydraulic performance of a hydraulic mining shovel radiator working with nanofluids is carried out. It is observed so far that there are no research works done before analyzing the radiator of this mining equipment. Aluminum oxide in ethylene glycol as nanofluid with volume concentrations of 0.5%, 1.0% and 1.5% were investigated. The results showed that the heat transfer performance of the radiator can be hindered if thermal operating parameters of the equipment are not varied to take advantage of the benefits done by nanofluids. Additionally, it has been found that the pressure drop performance on the radiator operating in laminar and transitional conditions can reduce pressure drop and therefore pumping power. The analysis presented in this paper concluded that the use of nanofluids essentially depends on thermal and flow conditions.

1. INTRODUCTION

An optimal thermal management for Internal Combustion Engines (ICEs) constitutes one of the most promising and low-cost solutions for the reduction of fuel consumption and for increasing engine efficiency [1]. With the help of the cooling system, the thermal state of the engine is kept stable throughout the range of load and speed regimes and the most suitable temperature is ensured, with which the most optimal economic and energy indices are achieved. So, the optimization of the cooling systems of the ICEs is still in constant development through the use of new technologies such as coolants, materials, or structure [2, 3].

The performance of automotive radiators has been studied for years; however, radiators used in mining equipment are overlooked since several unique factors are involved in their thermal analysis [4]. First, the variable heat loads of a machine operating on a dynamic cycle are difficult to predict accurately [5, 6]. Second, large industrial radiator development and design mainly rely on the empirical formula, which results in the shortcomings of long design cycles and high cost of testing, while using numerical computing technology can overcome these deficiencies [7]. By considering this, a higher efficiency can be obtained if the fin material has high thermal conductivity [8] and the use of an adequate finned surface increases the heat transfer performance in the heat exchanger [9]. Third, traditionally cooling systems of mining equipment use a mixture of ethylene glycol with water, since the higher temperatures of applications this mixture is used to elevate the aqueous boiling points [10]. The major use of ethylene glycol is as a medium for convective heat transfer in many practical and industrial components that require heating or cooling applications. Water is commonly used for automotive applications; however, the trouble with water is that it freezes or boils at extreme temperatures. Anti-freezing agents like ethylene glycol can withstand much greater temperature extremes [11, 12]. Also, it can be considered that the huge unsteady heat rejection and water pressure loads induce strong thermal stresses that become a critical issue for the design of these radiators and so on deteriorate some components of the cooling system [5].

Considerable attention has been given to nanofluids, nanoscale colloidal solutions, consisting of nanoparticles (with sizes of the order of 1 to 100 nm) dispersed in a base fluid [13]. When the nanoparticles are uniformly dispersed and added to the base fluids, the suspension of nanoparticles shows a dramatic enhancement in the thermal features of the base fluids [14, 15]. Different works in the literature have shown that the thermal execution of various heat systems can be improved by adopting various nanofluids with nanoparticles like Al_2O_3, CuO, Fe_2O_3, TiO_2 and carbon-based were used as additives of base fluids [16-25]. But also, organic nanofluids can be considered for future studies since they have a low environmental impact because they are recyclable and biodegradable [26]. Organic-based nanofluids are also believed to be less harmful to humans, animals, and aquatic organisms [27].

Among the nanoparticles before mentioned, Al_2O_3 is one of the most studied and commercially available. A numerical study simulated turbulent and laminar flow heat transfer in nanofluids (Al_2O_3 particles in water and ethylene glycol-based fluid) passing through a flat tube in 3D using computational fluid dynamics (CFD) for single and two-phase approaches. The results indicated that, for a given heat transfer rate, the required nanofluid volumetric flow rate was less than that for pure base fluid flow having a low pressure drop, decreasing the pumping power required [20]. An experimental study evaluated forced convective heat transfer in water-based Al_2O_3/nanofluid and pure water in an automobile radiator. The results indicated that at the concentration of 1 vol.%, the heat

transfer enhancement of 45% compared to pure water was recorded [21]. An experimental study on the performance of Al_2O_3/water-MEG based nanofluids as a car radiator coolant has been investigated. The results indicated that heat transfer rate by nanofluid coolant significantly increases with the increase in concentration of nanoparticles. For lowest coolant flow rate 4.06LPM as the volume fraction increases from 0.2-0.8% the enhancement in Nusselt number changes from 3.89% to 28.47% [22]. A numerical study investigated three different nanofluids: Al_2O_3, CuO and TiO_2. Among all three nanofluids, Al_2O_3 nanofluid shows the best thermal performance [23]. A review was performed on the use of water-based Al_2O_3 nanofluid as a heat transfer fluid. Gathered data showed the Nusselt number of the bulk fluid to increase by 50% with the introduction of 1% by volume of Al_2O_3 nanoparticles to the base fluid [24]. An experimental study of glycerin/Al_2O_3 nanofluid for automotive cooling applications. The results showed that significant enhancement in the convective heat transfer coefficient was observed in the laminar flow regime. The thermal enhancement increases with Reynolds number as well as particle concentrations. The effectiveness of the radiator increases as the particle concentration increases [25].

In his recent study working with alumina nanofluid, the authors [28] found out that the heat transfer performance increased with the increase of nanofluid concentration, and the heat transfer performance improvement was achieved higher for the low power tests (brake power). Also, a study working with alumina nanofluid found that 1% concentration in the nanofluid was able to reduce the coolant outlet temperature close to the generally recommended working conditions [29].

The present study presents a preliminary simulation effort on the performance of a hydraulic mining shovel radiator working with nanofluid. It is observed so far in the literature that have not been reported an analysis of this mining equipment. Therefore, a numerical study is carried out to present a heat transfer and pressure drop analysis at three different volume concentrations of Al_2O_3/Ethylene Glycol-Water nanofluid in this heat exchanger.

2. THERMOPHYSICAL PROPERTIES

Properties for density, specific heat, dynamic viscosity, and thermal conductivity of the base coolant fluid and nanofluids are required for the study. Studies have given us accurate data for the properties of these fluids. So, it is possible to obtain a relation between a temperature range suitable for this study and the thermophysical properties.

2.1 Conventional coolant properties

Traditional heavy-duty equipment coolant usually has a composition of a 50:50 ethylene glycol and water mixture. The base fluid properties data were obtained from the ASHRAE Fundamentals Handbook [30] and curve fitted as a function of temperature, over a range of 60°C ≤ T ≤ 120°C that will be encountered by an internal combustion engine cooling system. The thermophysical correlations of the base coolant fluid presented in Table 1 show a coefficient of determination $R^2 \approx 1$.

Table 1. EG/W 50:50 properties correlation for 60°C ≤ T ≤ 120°C

Property	Correlation	R^2	Equation
Density (kg/m^3)	$\rho = -0.0024T^2 - 0.3381T + 1081.1$	1	(1)
Viscosity (Pa.s)	$\mu = 0.0037e^{-0.017T}$	0.996	(2)
Specific heat (J/kg-K)	$c = 3.8616T + 3203.4$	1	(3)
Thermal conductivity (W/m-°C)	$k = -3\cdot10^{-6}T^2 + 0.0008T + 0.3526$	0.999	(4)

2.2 Nanofluid properties

Although experiments and studies of nanofluids have been carried out, there is no comprehensive review on nanofluids properties from various aspects [31, 32]. We can consider some studies done to obtain these properties. The following correlations have been used to predict nanofluid density and specific heat, respectively, at different temperatures and concentrations [33, 34].

$$\rho_{nf} = \phi\rho_p + (1-\phi)\rho_{bf} \tag{5}$$

$$(\rho c)_{nf} = \phi(\rho c)_p + (1-\phi)(\rho c)_{bf} \tag{6}$$

Correlations for thermal conductivity and viscosity for ethylene glycol – Al_2O_3 were developed by Chiam et al. [35] considering the study done by Sundar et al. [36].

$$\frac{k_{nf}}{k_{bf}} = 0.9683(1+\phi)^{11.13}\left(1+\frac{T}{70}\right)^{0.1676}(0.01+BR)^{0.00111} \tag{7}$$

$$\frac{\mu_{nf}}{\mu_{bf}} = (1+\phi)^{32}\left(\frac{T}{70}\right)^{-0.001}(0.1+BR)^{0.08} \tag{8}$$

3. HYDRAULIC MINING SHOVEL RADIATOR

The heavy-duty equipment analyzed in this study is a hydraulic mining shovel shown in Figure 1. It has two internal combustion engines located at the rear of the vehicle (To the right side on Figure 1). Figure 2 shows the ICE with the radiators. In Table 2 are shown the specifications of each ICE.

Table 2. Specifications of the internal combustion engine

Parameter	Engine
Configuration	V12
Maximum Power (kW)	2256
Rated Speed Max. Power (RPM)	1800
Maximum Torque (Nm)	14755
Rated Speed Max. Torque (RPM)	1350

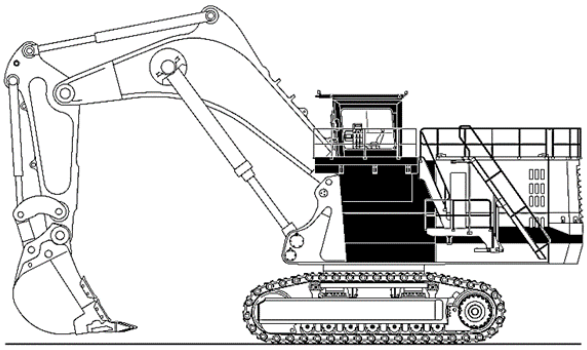

Figure 1. Hydraulic mining shovel

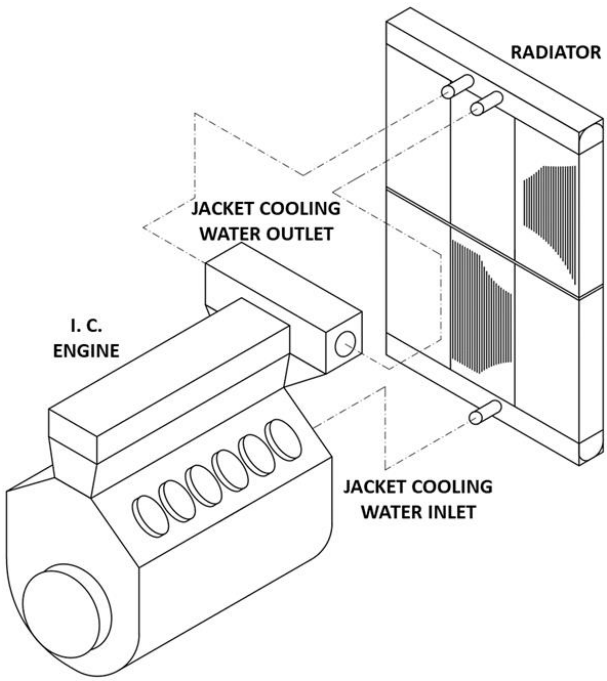

Figure 2. Schematic of internal combustion engine with the radiator

3.1 Surface geometries

The radiators are made of aluminum. Table 3 lists the structural parameters and Table 4 the dimensions of the radiator with their values needed for the analysis of the performance of this radiator. The schematic geometry of the radiator is shown in Figure 3(a). In Figure 3(b) and 3(c) are shown schematics for structural parameters of water-side and air-side, respectively.

Table 3. Structural parameters of compact aluminum radiator

Parameter	Symbol	Water side	Air side
Fin configuration	-	Offset Strip	Plain
Fin Thickness (mm)	t	0.5	0.5
Fin Height (mm)	h	6.4	9.2
Plate spacing (mm)	b	6.9	9.7
Fin Length (mm)	l	6.0	139.7
Fin spacing (mm)	s	4.6	4.4
Plate thickness (mm)	a	0.8	0.8

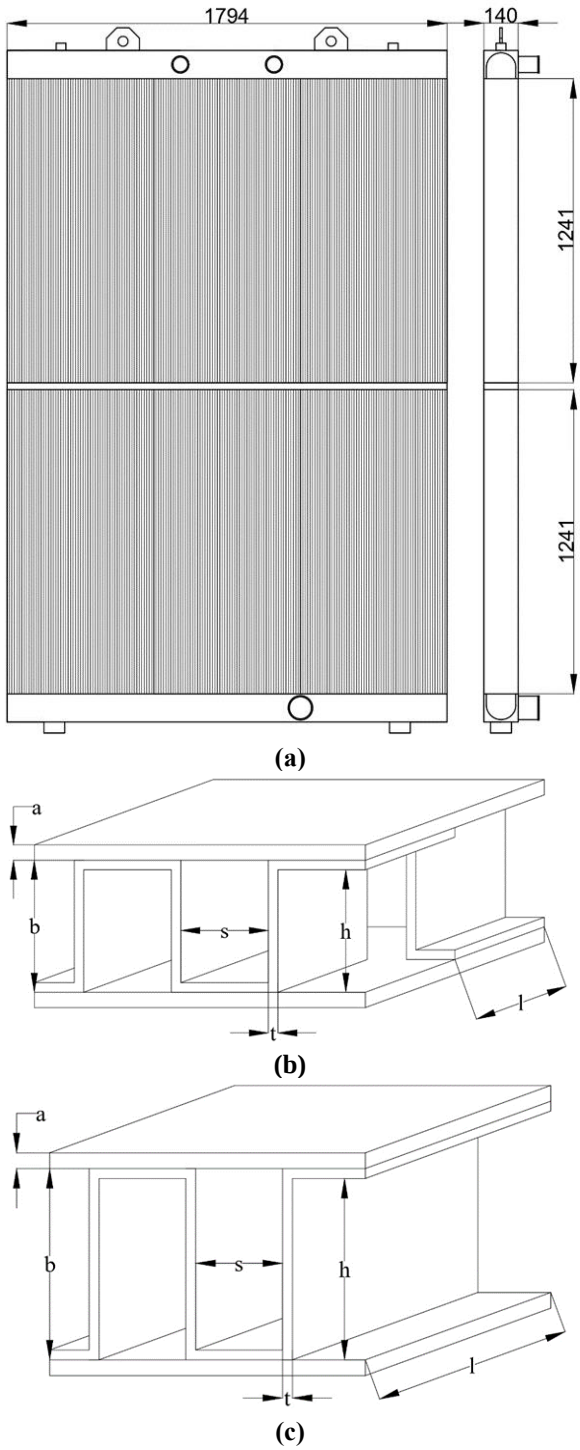

Figure 3. Schematic geometry of the radiator

Table 4. Dimensions of the radiator

Parameter	Symbol	Value
Length (mm)	L	2482
Width (mm)	W	1794
Height (mm)	H	140

3.2 Equations for surface geometries

Additional surface geometries are required for the air and coolant sides to analyze the performance of the radiator. The equations shown in Table 5 show how these geometries were calculated [37].

Table 5. Equations for surface geometries

Parameter	Formula	Equation
Hydraulic radius; r_h (m^2)	$r_h = \frac{D_h}{4}$	(9)
Frontal Area; A_{fr} (m^2)	$A_{fr,a} = LW, A_{fr,c} = WH$	(10)
Total transfer area/volume between plates: β (m^2/m^3)	$\beta = \frac{2(hl + sl + ht)}{bl(s+t)}$	(11)
Total transfer area/total exchanger volume: α (m^2/m^3)	$\alpha = \frac{\beta b}{b_1 + b_2 + 2a}$	(12)
Free flow area/frontal area: σ	$\sigma = r_h \alpha$	(13)
Fin surface area/Total transfer area: φ	$\varphi = \frac{h(l+t)}{(hl + sl + ht)}$	(14)

Volume of the radiator; V (m^3):

$$V = LWH \tag{15}$$

Hydraulic diameter; Dh (m^2)
Air side

$$D_{h,a} = \frac{2 s_a h_a}{s_a + h_a} \tag{16}$$

Coolant side

$$D_{h,c} = \frac{2 l_c h_c (s_c - t_c)}{l_c h_c + l_c s_c + h_c t_c} \tag{17}$$

4. HEAT TRANSFER ANALYSIS

4.1 Operational parameters selected as inputs

Hydraulic mining shovel is part of a large number of heavy-duty equipment. They usually work in off-highway conditions such as mining or construction. The operational conditions of these heavy-duty radiators, such as inlet and outlet temperatures and flow rates for both coolant and air, must be used to compare performance of the radiator using different fin configurations and coolants.

Table 6. Operational conditions for heavy-duty radiators

Parameter	Sources [4,5,7]		Parameters used for this study
	Min	Max	
Air Inlet Temperature (°C)	41	43	40
Air Outlet Temperature (°C)	69	72	70
Coolant Inlet Temperature (°C)	89	92	90
Coolant Outlet Temperature (°C)	80	83	80
Coolant mass flow rate (kg/s)	6	62	10-50

These data were collected from studies done before and are summarized in Table 6 along with the current testing conditions. It also depends on the operation and speed of the ICE. The parameters used for this study are also shown. These data were obtained by Engine Control Module (ECM) system from the shovel that can be connected to a computer and digitally obtain its operational parameters.

4.2 Equations for heat transfer analysis

Since this radiator is a compact heat exchanger, we can considerer the heat balance in the air-side and the coolant-side as follows in Eq. (18).

$$Q = \dot{m}_c c_c (T_{c,o} - T_{c,i}) = \dot{m}_a c_a (T_{a,i} - T_{a,o}) \tag{18}$$

The mass velocity and Reynolds number on both sides is evaluated in Eqns. (19) and (20). The mass velocity is considered per unit, on both sides per fin spacing.

$$G = \frac{\dot{m}_{unit}}{A_{unit}} \tag{19}$$

$$\mathrm{Re} = \frac{D_h G}{\mu} \tag{20}$$

4.2.1 Equations for the coolant side

For laminar flow, Shah and London [38] presented two equations of heat transfer under constant axial wall heat flux for developing laminar flows (Re<2300) for a single-phase liquid.

$$Nu_{lam} = 1.953 \left(\mathrm{Re}_c \, \mathrm{Pr}_c \frac{D_{h,c}}{L} \right)^{1/3} \quad for \quad \left(\mathrm{Re}_c \, \mathrm{Pr}_c \frac{D_{h,c}}{L} \right) \geq 33.33 \tag{21}$$

$$Nu_{lam} = 4.364 + 0.0722 \left(\mathrm{Re}_c \, \mathrm{Pr}_c \frac{D_{h,c}}{L} \right) \quad for \quad \left(\mathrm{Re}_c \, \mathrm{Pr}_c \frac{D_{h,c}}{L} \right) < 33.33 \tag{22}$$

For turbulent flow, Gnielinkski [39] developed an equation taking into consideration that the friction factor for turbulent flow that was defined by Vajjha et al. [40] in Eq. (35).

$$Nu_{turb} = \frac{(f_{turb}/8)(\mathrm{Re}_c - 1000)\,\mathrm{Pr}_c}{1 + 12.7\sqrt{(f_{turb}/8)}\,(\mathrm{Pr}_c^{2/3} - 1)} \times [1 + \left(\frac{D_{h,c}}{L} \right)^{2/3}] \left(\frac{\mathrm{Pr}_c}{\mathrm{Pr}_w} \right)^{0.11} \tag{23}$$

For the transitional flow, Gnielinski [41] developed a practical approach for a Nusselt Number correlation in the transitional region (2300<Re<~3000). In Eq. (24) is shown that correlation, the laminar Nusselt Number is calculated by Eq. (21) and (22), and the turbulent Nusselt Number is calculated by Eq. (23).

$$Nu_{tran} = (1-\gamma)Nu_{lam,2300} + \gamma Nu_{turb,4000} \tag{24}$$

With

$$\gamma = \frac{\mathrm{Re}_c - 2300}{4000 - 2300} \quad and \quad 0 \le \gamma \le 1 \tag{25}$$

Coolant-side convective heat transfer coefficient is shown in Eq. (26):

$$h_c = \frac{Nu_c k_c}{D_{h,c}} \tag{26}$$

4.2.2 Equations for the air side

A correlation was developed for the Colburn Factor by curvefitting the data from Kays and London [37] on plain plate fin surface 6.2 which one meets with the structural parameters shown in Table 3. It is shown in Table 7. Air-side convective heat transfer coefficient is shown in Eq. (27).

$$h_a = \frac{j_a G_a c_a}{\mathrm{Pr}_a^{2/3}} \tag{27}$$

4.2.3 Equations for heat transfer performance of the radiator

Surface effectiveness of the fins is part of the heat transfer coefficient balance, it is calculated with fin efficiency shown in Eq. (30) and Fin area divided by the total area relation.

$$m_f = \sqrt{\frac{2h_a}{k_{Al}t}} \tag{28}$$

$$\eta_f = \frac{\tanh(m_f(h+t))}{m_f(h+t)} \tag{29}$$

$$\eta_o = 1 - \frac{A_f}{A_T}(1-\eta_f) \tag{30}$$

Overall heat transfer coefficient in the air-side:

$$\frac{1}{U_a} = \frac{1}{\eta_{0,a}h_a} + \frac{1}{\left(\frac{\alpha_c}{\alpha_a}\right)\eta_{0,c}h_c} \tag{31}$$

4.3 Equations for pressure drop analysis

A theoretical relation for single phase fluid pressure drop can be expressed as follows in Eq. (32):

$$\Delta P = \frac{fL_r G^2}{2D_h \rho} \tag{32}$$

4.3.1 Equations for the coolant side

For the laminar flow, Hwang et al. [42] studied the friction factor of water-based Al_2O_3 nanofluids flowing through a tube by analyzing the pressure drop. Results shown that the Darcy friction factor in fully developed laminar flow regime has a good agreement with Eq. (33).

$$f_{lam} = \frac{64}{\mathrm{Re}_c} \tag{33}$$

However, Sharma et al. [43] indicated that the Brownian motion and random collisions between the nanoparticles at higher concentrations could result in higher friction factors in comparison to the base fluid or nanofluid with low concentrations (ϕ <0.5%). They studied the pressure drop in laminar flow through a tube by using EG:W-based Al_2O_3 nanofluids. They proposed the correlation shown in Eq. (34) considering the nanofluid concentration

$$f_{lam} = \frac{64}{\mathrm{Re}_c}\left[1 + 2.55\left(\frac{\phi}{1-\phi}\right)^{0.70}\right] \tag{34}$$

For the turbulent flow, Vajjha et al. [40] developed a correlation for this regime shown in Eq. (35) by considering the density and viscosity variation between nanofluid and basefluid.

$$f_{turb} = 0.3164\,\mathrm{Re}_c^{-0.25}\left(\frac{\rho_{nf}}{\rho_{bf}}\right)^{0.797}\left(\frac{\mu_{nf}}{\mu_{bf}}\right)^{0.108} \tag{35}$$

For the transitional flow, as well as in the heat transfer analysis, the practical approach done by Gnielinski [41] fits in the pressure drop analysis

$$f_{tran} = (1-\gamma)f_{lam,2300} + \gamma f_{turb,4000} \tag{36}$$

With

$$\gamma = \frac{\mathrm{Re}_c - 2300}{4000 - 2300} \quad and \quad 0 \le \gamma \le 1 \tag{37}$$

Table 7. Colburn and friction factor correlations for the air-side

Reynolds Number	Correlation	R^2	Equation
800<Re<3000	$j_a = 1.1\cdot10^{-9}\,\mathrm{Re}_a^{\,2} - 5.3\cdot10^{-6}\,\mathrm{Re}_a + 0.0092$	0.993	(38)
3000<Re<4000	$j_a = -5\cdot10^{-11}\,\mathrm{Re}_a^{\,2} + 4.2\cdot10^{-7}\,\mathrm{Re}_a + 0.00245$	1	(39)
4000<Re<12000	$j_a = -3.8\cdot10^{-8}\,\mathrm{Re}_a + 0.00348$	0.998	(40)
800<Re<2500	$f_a = 5.1\cdot10^{-9}\,\mathrm{Re}^2 - 2.3\cdot10^{-5}\,\mathrm{Re} + 0.03604$	0.995	(41)
2500<Re<12000	$f_a = 2.4\cdot10^{-11}\,\mathrm{Re}_a^{\,2} - 5.9\cdot10^{-7}\,\mathrm{Re}_a + 0.0108$	0.993	(42)

4.3.2 Equations for the air side

A correlation was developed for the Colburn Factor by curve fitting the data from Kays and London [37] on plain plate fin surface 6.2 which one meets with the structural parameters shown in Table 3. It is shown in Table 7.

5. RESULTS

In this section, the heat transfer and pressure drop performance of a hydraulic mining shovel radiator is developed considering the air-side overall heat transfer coefficient versus the air Reynolds number, the coolant convective heat transfer coefficient versus the coolant Reynolds number, the air-side pressure drop versus the air Reynolds number, and the coolant-side pressure drop versus the coolant Reynolds number.

The effects of volumetric concentration of nanoparticles on the performance of nanofluids are examined in Figures 4, 5 and 7. It is noted in the nanofluid literature that increasing particle concentration increases thermal conductivity and viscosity. An increase in thermal conductivity will increase the convection coefficient if the Nusselt number is maintained the same. While an increase in viscosity will increase the Prandtl number but decrease the Reynolds number influencing heat transfer [15, 44]

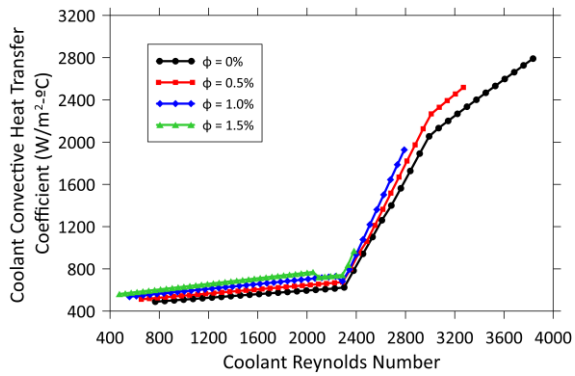

Figure 4. Coolant convective heat transfer coefficient versus the coolant Reynolds number

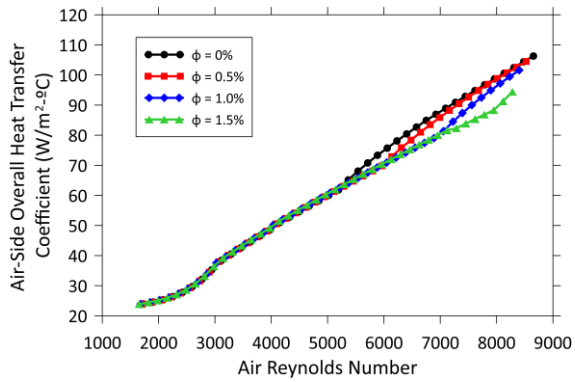

Figure 5. Air-side overall heat transfer coefficient vs the air Reynolds number

5.1 Heat transfer performance

The effect of the coolant convective heat transfer coefficient per Al_2O_3 nanofluid volume concentration is shown in Figure 4. Under equal heat dissipation, nanofluids will perform at a much lower Reynolds number and so on at a lower heat transfer coefficient. With a 0.5% concentration we see the Reynolds number drop as much as 18% compared to the base fluid (volume concentration of 0%). Increasing the particle volume concentration to 1.0% or 1.5% will continue to lower the nanofluids Reynolds number due to the increase in viscosity of the fluid.

Optimal volume concentration for convective heat transfer coefficient on the coolant-side depends on the coolant regime. The nanofluid literature shows that the heat transfer coefficient strongly depends on nanoparticles concentration. It is also higher for higher Reynolds number. That means turbulent flow conditions are more feasible in comparison to laminar flow for nanofluids [45]. In the present study, the radiator working only with the basefluid, has a coolant Reynolds number in a range of 767 to 3836 that is part of laminar, transitional and turbulent flow. With a volume concentration of 0.5%, the coolant Reynolds number in a range of 654 to 3270 that is part of laminar, transitional and turbulent flow. With a volume concentration of 1.0%, the coolant Reynolds number is in a range of 558 to 2790 that is part of laminar and transitional flow. With a volume concentration of 1.5%, the coolant Reynolds number in a range of 476 to 2382 that is part of laminar and transitional flow. So that, the optimal volume concentration for convective heat transfer coefficient is in the range of 0% to 0.5%. However, the difference done by increasing the volume concentration in that range is not very notable in this heat exchanger, since the coolant Reynolds number in the turbulent flow is still lower.

The effect of the air-side overall heat transfer coefficient per Al_2O_3 nanofluid volume concentration is shown in Figure 5. The air Reynolds number plays a more vital role when looking at overall heat transfer coefficient. Note that the air-side overall heat transfer coefficient is the same independently of the volume concentration until the air Reynolds number of 5250.

Then, the overall heat transfer coefficient has different values considering the volume concentration, since the coolant is varying from laminar flow to transitional flow and so on to turbulent flow as mentioned before. Working with a nanofluid volume concentration of 0% and 0.5%, the coolant reaches the turbulent regime and so that the overall heat transfer coefficient on the air-side is higher than by working with a nanofluid volume concentration of 1.0% and 1.5%.

As mentioned before, the process is under constant wall heat flux. Also, since the cooling system of the hydraulic shovel is controlled by Engine Control Module (ECM) system, the inlet and outlet temperatures are determined by the equipment and could not be changed since it could provoke power losses in the ICE.

5.2 Pressure drop performance

The effect of the air-side pressure drop is shown in Figure 6. There is no variation in the pressure drop on the air side since the concentration of the nanofluid volume does not influence in this case, since this trend only depends on the Reynolds number of the air.

As we can see, the pressure drop is lower than 100 Pa; that is very much lower than atmospheric pressure. The geometry on the air-side is plain plate fin, so that by using a different geometry such as louvered or staggered, can improve the fin efficiency of the heat exchanger and so on the heat transfer performance.

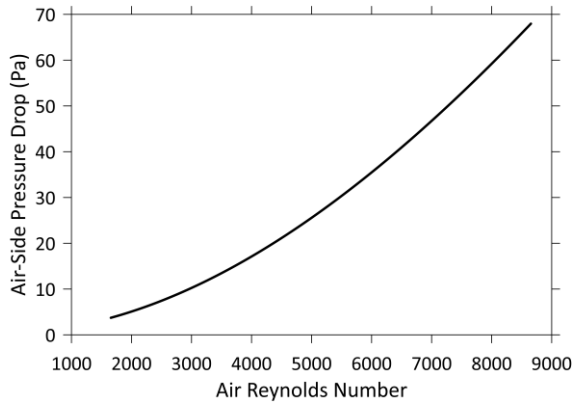

Figure 6. Air-side pressure drop versus the air Reynolds number

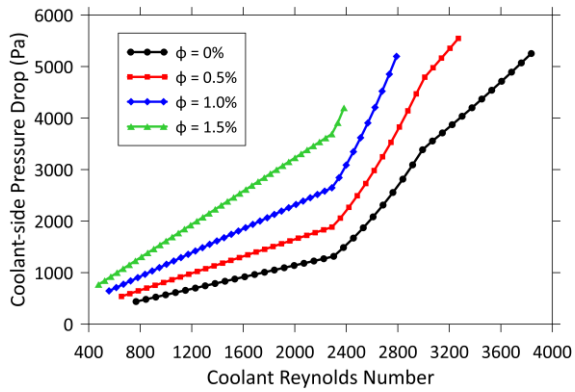

Figure 7. Coolant-side pressure drop versus the coolant Reynolds number

The effect of the coolant-side pressure drop per Al_2O_3 nanofluid volume concentration is shown in Figure 7. For a higher coolant Reynolds number its seen that there is a higher pressure drop, as expected (enhanced viscosity); it increases as the nanofluid volume concentration also increases. The radiator working only with the basefluid, has a pressure drop in a range of 438 to 5253 Pa that is part of laminar, transitional and turbulent flow. With a volume concentration of 0.5%, the coolant Reynolds number in a range of 538 to 5546 Pa that is part of laminar, transitional and turbulent flow. With a volume concentration of 1.0%, the coolant Reynolds number in a range of 645 to 5198 Pa that is part of laminar and transitional flow. With a volume concentration of 1.5%, the coolant Reynolds number in a range of 769 to 4198 Pa that is part of laminar and transitional flow.

6. CONCLUSIONS

In this paper, it is shown the heat transfer and pressure drop performance of a hydraulic mining shovel radiator by using ethylene glycol/water-based Al_2O_3 nanofluids that has been numerically analyzed. The following are the key findings of this study:

- The thermal design of the radiator is not adequate since the geometry both on the air-side and coolant-side could be improved [8]. Also, the material of the radiator could be changed, considering that the hydraulic mining shovel works under heavy-duty conditions; the maintenance of the radiator is more feasible if it is made of copper [4].
- The performance of heat transfer by using nanofluid should be analyzed considering the engine and the cooling system, since this type of machinery expels large amounts of heat through the radiator. Therefore, in order to take advantage of the benefits done by nanofluids, the thermal operating parameters of the motor assembly must be varied. So that, in this study, fluid properties and geometry of the radiator can hinder the performance of basefluid [44].
- As we can see, for lower coolant flow rates and lower nanofluid volume concentrations, the pressure drop is lower. But for higher coolant flow rates and lower concentrations, the pressure drop is higher. It means that heat exchangers operating in laminar and transitional conditions can reduce pressure drop and therefore pumping power.

It is recommended that for a future study a test bench can be developed for these types of heat exchangers, by also considering the environment and vibrations of the off-highway conditions where this equipment is working.

REFERENCES

[1] Castiglione, T., Pizzonia, F., Bova, S. (2016). A novel cooling system control strategy for internal combustion engines. SAE International Journal of Materials and Manufacturing, 9(2): 294-302. https://doi.org/10.4271/2016-01-0226

[2] Heywood, J.B. (2018). Internal Combustion Engine Fundamentals. McGraw-Hill, New York.

[3] Kalelı, A., Kaltakkiran, G., Dumlu, A., Ayten, K. (2017). Design and control of intelligent cooling system for IC engine. 2017 International Conference on Engineering and Technology (ICET), pp. 1-3. https://doi.org/10.1109/ICEngTechnol.2017.8308163

[4] Canazas, J. (2021). Field study on the air-side heat transfer performance of copper finned-flat tubes for heavy-duty truck radiators. International Journal of Heat and Technology, 39(5): 1451-1459. https://doi.org/10.18280/ijht.390506

[5] Mao, S., Cheng C., Li, X., Michaelides, E. (2010). Thermal/structural analysis of radiators for heavy-duty trucks. Applied Thermal Engineering, 30(11-12): 1438-1446. https://doi.org/10.1016/j.applthermaleng.2010.03.003

[6] Borman, G., Nishiwaki, K. (1987). Internal-combustion engine heat transfer. Progress in Energy and Combustion Science, 13(1): 1-46. https://doi.org/10.1016/0360-1285(87)90005-0

[7] Fan, Z.J., Gu, Z.Q., Liu, S.C. (2012). Prediction of heat dissipation effect by simulating radiator group of mining dump-truck. Applied Mechanics and Materials, 217-219: 2473-2479. https://doi.org/10.4028/www.scientific.net/amm.217-219.2473

[8] Saha, S.K., Ranjan, H., Emani, M.S., Bharti, A.K. (2020). Heat transfer enhancement in externally finned tubes and internally finned tubes and annuli. Springer Briefs in Applied Sciences and Technology. https://doi.org/10.1007/978-3-030-20748-9

[9] Webb, R.L. (1980). Air-side heat transfer in finned tube heat exchangers. Heat Transfer Engineering, 1(3): 33-49. https://doi.org/10.1080/01457638008939561

[10] Sekrani, G., Poncet, S. (2018). Ethylene- and propylene-glycol based nanofluids: A literature review on their thermophysical properties and thermal performances. Applied Sciences, 8(11): 2311. https://doi.org/10.3390/app8112311

[11] Peyghambarzadeh, S.M., Hashemabadi, S.H., Hoseini, S.M., Seifi Jamnani, M. (2011). Experimental study of heat transfer enhancement using water/ethylene glycol based nanofluids as a new coolant for car radiators. International Communications in Heat and Mass Transfer, 38(9): 1283-1290. https://doi.org/10.1016/j.icheatmasstransfer.2011.07.001

[12] Gollin, M., Bjork, D. (1996). Comparative performance of ethylene glycol/water and propylene glycol/water coolants in automobile radiators. SAE Technical Paper Series. https://doi.org/10.4271/960372

[13] Taylor, R., Coulombe, S., Otanicar, T., Phelan, P., Gunawan, A., Lv, W., Rosengarten, G., Prasher, R., Tyagi, H. (2013). Small particles, big impacts: A review of the diverse applications of nanofluids. Journal of Applied Physics, 113(1): 011301. https://doi.org/10.1063/1.4754271

[14] Bhatti, M.M. (2021) Recent trends in nanofluids. Inventions, 6(2): 39. https://doi.org/10.3390/inventions6020039

[15] Cheng, L., Bandarra Filho, E.P., Thome, J.R. (2008). Nanofluid two-phase flow and thermal physics: a new research frontier of nanotechnology and its challenges. Journal of Nanoscience and Nanotechnology, 8(7): 3315-3332. https://doi.org/10.1166/jnn.2008.413

[16] Leong, K.Y., Saidur, R., Kazi, S.N., Mamun, A.H. (2010). Performance investigation of an automotive car radiator operated with nanofluid-based coolants (nanofluid as a coolant in a radiator). Applied Thermal Engineering, 30(17-18): 2685-2692. https://doi.org/10.1016/j.applthermaleng.2010.07.019

[17] Huminic, G., Huminic, A. (2017). Numerical analysis of hybrid nanofluids as coolants for automotive applications, International Journal of Heat and Technology, 35(1): S288-S292. https://doi.org/10.18280/ijht.35Sp0139

[18] Ravisankar, R. (2018). Application of nanotechnology to improve the performance of tractor radiator using cu-water nanofluid. Journal of Thermal Engineering, 4(4): 2188-2200. https://doi.org/10.18186/journal-of-thermal-engineering.434036

[19] Madderla, S., Ramasamy, D., Sudhakar, K., Kadirgama, K., Wan Harun, W.S. (2021). Heat transfer performance of a radiator with and without louvered strip by using Graphene-based nanofluids. Journal of Thermal Engineering, 7(6): 1315-1328. https://doi.org/10.18186/thermal.989959

[20] Delavari, V., Hashemabadi, S.H. (2014). CFD simulation of heat transfer enhancement of Al_2O_3/water and Al_2O_3/ethylene glycol nanofluids in a car radiator. Applied Thermal Engineering, 73(1): 380-390. https://doi.org/10.1016/j.applthermaleng.2014.07.061

[21] Peyghambarzadeh, S.M., Hashemabadi, S.H., Jamnani, M.S., Hoseini, S.M. (2011). Improving the cooling performance of automobile radiator with Al_2O_3/water nanofluid. Applied Thermal Engineering, 31(10): 1833-1838. https://doi.org/10.1016/j.applthermaleng.2011.02.029

[22] Subhedar, D.G., Ramani, B.M., Gupta, A. (2018). Experimental investigation of heat transfer potential of Al_2O_3 /Water-Mono Ethylene Glycol nanofluids as a car radiator coolant. Case Studies in Thermal Engineering, 11: 26-34. https://doi.org/10.1016/j.csite.2017.11.009

[23] Hafeez, M.B., Amin, R., Nisar, K.S., Jamshed, W., Abdel-Aty, A.H., Khashan, M.M. (2021). Heat transfer enhancement through nanofluids with applications in automobile radiator. Case Studies in Thermal Engineering, 27: 101192. https://doi.org/10.1016/j.csite.2021.101192

[24] Issa, R.J. (2021). Automobile radiator integrated with Al2O3 nanofluid for compact size and sustainability enhancement. International Journal of Heat and Technology, 39(4): 1057-1065. https://doi.org/10.18280/ijht.390403

[25] Sundari, K.G., Asirvatham, L.G., Marshal S., J.J., Ninolin, E., B., S. (2020). Feasibility of glycerin/Al_2O_3 nanofluid for automotive cooling applications. Journal of Thermal Engineering, 6(4): 619-632. https://doi.org/10.18186/thermal.766416

[26] Amin, A., Hamzah, W., Oumer, A. (2021). Thermal conductivity and dynamic viscosity of mono and hybrid organic- and synthetic-based nanofluids: A critical review. Nanotechnology Reviews, 10(1): 1624-1661. https://doi.org/10.1515/ntrev-2021-0086

[27] Sharifpur, M., Solomon, A.B., Meyer, J.P., Ibrahim, J.S., Immanuel, B. (2017). Thermal conductivity and viscosity of mango bark/water nanofluids. 13th International Conference on Mechanics and Thermodynamics. Portoroz, Slovenia.

[28] Karagöz, Y., Köten, H., Tunçer, E., Pusat, S. (2022) Effect of Al_2O_3 addition to an internal combustion engine coolant on heat transfer performance. Case Studies in Thermal Engineering, 31: 101847. https://doi.org/10.1016/j.csite.2022.101847

[29] Anis, S., Kayunda, Y., Kusumastuti, A., Simanjutak, J. (2022). Simulation study of Al_2O_3 -H_2O nanofluids as radiator coolant using computational fluid dynamics method. IOP Conference Series: Earth and Environmental Science, 969: 012026. https://doi.org/10.1088/1755-1315/969/1/012026

[30] ASHRAE. (2017). ASHRAE Handbook: Fundamentals. American Society of Heating, Refrigerating and Air-Conditioning Engineers, Atlanta, GA.

[31] Li, J., Zhang, X., Xu, B., Yuan, M. (2021). Nanofluid research and applications: A review. International Communications in Heat and Mass Transfer, 127: 105543. https://doi.org/10.1016/j.icheatmasstransfer.2021.105543

[32] Sheikh, N.A., Chuan Ching, D.L., Khan, I. (2020). A comprehensive review on theoretical aspects of nanofluids: exact solutions and analysis. Symmetry, 12(5): 725. https://doi.org/10.3390/sym12050725

[33] Pak, B.C., Cho, Y.I. (1998). Hydrodynamic and heat transfer study of dispersed fluids with submicron metallic oxide particles. Experimental Heat Transfer, 11(2): 151-170. https://doi.org/10.1080/08916159808946559

[34] Xuan, Y., Roetzel, W. (2000). Conceptions for heat transfer correlation of nanofluids. International Journal of Heat and Mass Transfer, 43(19): 3701-3707. https://doi.org/10.1016/s0017-9310(99)00369-5

[35] Chiam, H.W., Azmi, W.H., Usri, N.A., Mamat, R., Adam, N.M. (2017). Thermal conductivity and viscosity of Al_2O_3 nanofluids for different based ratio of water and ethylene glycol mixture. Experimental Thermal and Fluid Science, 81: 420-429. https://doi.org/10.1016/j.expthermflusci.2016.09.013

[36] Syam Sundar, L., Venkata Ramana, E., Singh, M.K., Sousa, A.C.M. (2014). Thermal conductivity and viscosity of stabilized ethylene glycol and water mixture Al_2O_3 nanofluids for heat transfer applications: An experimental study. International Communications in Heat and Mass Transfer, 56: 86-95. https://doi.org/10.1016/j.icheatmasstransfer.2014.06.009

[37] Kays, W.M., London, A.L. (1998). Compact Heat Exchangers. KriegerPub. Co., Malabar, FL.

[38] Shah, R.K., London, A.L. (1978). Laminar Flow Forced Convection in Ducts. Academic Press, New York.

[39] Gnielinski, V. (1975). Neue Gleichungen für den Wärme- und den Stoffübergang in turbulent durchströmten Rohren und Kanälen. Forschung Im Ingenieurwesen, 41(1): 8-16. https://doi.org/10.1007/bf02559682

[40] Vajjha, R.S., Das, D.K., Kulkarni, D.P. (2010). Development of new correlations for convective heat transfer and friction factor in turbulent regime for nanofluids. International Journal of Heat and Mass Transfer, 53(21-22): 4607-4618. https://doi.org/10.1016/j.ijheatmasstransfer.2010.06.032

[41] Gnielinski, V. (2013). On heat transfer in tubes. International Journal of Heat and Mass Transfer, 63: 134-140. https://doi.org/10.1016/j.ijheatmasstransfer.2013.04.015

[42] Hwang, K.S., Jang, S.P., Choi, S.U.S. (2009). Flow and convective heat transfer characteristics of water-based Al_2O_3 nanofluids in fully developed laminar flow regime. International Journal of Heat and Mass Transfer, 52(1-2): 193-199. https://doi.org/10.1016/j.ijheatmasstransfer.2008.06.032

[43] Sharma, P., Gupta, R., Wanchoo, R.K. (2017). Hydrodynamic studies on glycol based Al_2O_3 nanofluid flowing through straight tubes and coils. Experimental Thermal and Fluid Science, 82: 19-31. https://doi.org/10.1016/j.expthermflusci.2016.11.001

[44] Ray, D.R., Das, D.K. (2014). Superior performance of nanofluids in an automotive radiator. Journal of Thermal Science and Engineering Applications, 6(4): 041002. https://doi.org/10.1115/1.4027302

[45] Kumar, P., Pandey, K.M. (2017). Effect on heat transfer characteristics of nanofluids flowing under laminar and turbulent flow regime – a review. IOP Conference Series: Materials Science and Engineering, 225: 012168. https://doi.org/10.1088/1757-899x/225/1/012168

NOMENCLATURE

t	fin thickness, mm
h	fin height, mm
b	plate spacing, mm
l	fin length, mm
s	fin spacing, mm
a	plate thickness, mm
D	diameter, mm
r	radius, mm
L	length, mm
W	width, mm
H	height, mm
A	area, m^2
BR	base mixture ratio
V	volumetric flow, m^3/s
m	mass flow, kg/s
Q	heat transfer rate, W
c	specific heat, J/(kg-°C)
k	thermal conductivity, (W/m-°C)
T	temperature, °C
h	convective coefficient, W/(m^2-°C)
G	mass air flow, kg/s-m^2
Re	Reynolds number
Pr	Prandtl number
Nu	Nusselt number
U	overall heat transfer coefficient, W/(m^2-°C)
f	Friction factor
j	Colburn factor
ΔP	pressure drop, Pa

Greek symbols

α	total transfer area/total exchanger volume, m^2/m^3
β	total transfer area/volume between plates, m^2/m^3
ρ	density, m^3/kg
η	efficiency, %
μ	dynamic viscosity, Pa.s
σ	free flow area/frontal area
φ	fin surface area/Total transfer area
ϕ	nanofluid volume concentration
γ	intermittency factor

Subscripts

fr	frontal
c	coolant side
a	air side
h	hydraulic parameter
nf	nanofluid
bf	basefluid
p	particle
lam	laminar regime
turb	turbulent regime
tran	transitional regime